EFDA–JET–PR(12)38

S. Saarelma, M.N.A. Beurskens, D. Dickinson, L. Frassinetti, M.J. Leyland
C.M. Roach and JET EFDA contributors

MHD and Gyro-Kinetic Stability of JET Pedestals

"This document is intended for publication in the open literature. It is made available on the understanding that it may not be further circulated and extracts or references may not be published prior to publication of the original when applicable, or without the consent of the Publications Officer, EFDA, Culham Science Centre, Abingdon, Oxon, OX14 3DB, UK."

"Enquiries about Copyright and reproduction should be addressed to the Publications Officer, EFDA, Culham Science Centre, Abingdon, Oxon, OX14 3DB, UK."

The contents of this preprint and all other JET EFDA Preprints and Conference Papers are available to view online free at www.iop.org/Jet. This site has full search facilities and e-mail alert options. The diagrams contained within the PDFs on this site are hyperlinked from the year 1996 onwards.

MHD and Gyro-Kinetic Stability of JET Pedestals

S. Saarelma[1], M.N.A. Beurskens[1], D. Dickinson[1], L. Frassinetti[2], M.J. Leyland[3]
C.M. Roach[1] and JET EFDA contributors*

JET-EFDA, Culham Science Centre, OX14 3DB, Abingdon, UK

[1]EURATOM-CCFE Fusion Association, Culham Science Centre, OX14 3DB, Abingdon, OXON, UK
[2]Division of Fusion Plasma Physics, School of Electrical Engineering, Royal Institute of Technology, Association EURATOM-VR, Stockholm, Sweden
[3]York Plasma Institute, Dept. of Physics, University of York, York, YO10 5DD, UK
** See annex of F. Romanelli et al, "Overview of JET Results", (24th IAEA Fusion Energy Conference, San Diego, USA (2012)).*

Preprint of Paper to be submitted for publication in
Nuclear Fusion

ABSTRACT

The pedestal profile measurements in high triangularity JET plasmas show that with low fuelling the pedestal width decreases during the ELM cycle and with high fuelling it stays constant. In the low fuelling case the pedestal pressure gradient keeps increasing until the ELM crash and in the low fuelling case it reaches a saturation during the ELM cycle.

An edge stability analysis using MHD and gyro-kinetic codes finds that at the end of the ELM cycle both JET plasmas become limited by finite-n peeling-ballooning modes and during the ELM cycle the steep pressure gradient region of the pedestal is both n = 1 ideal MHD ballooning mode and kinetic ballooning mode stable due to high bootstrap current. This indicates that during the ELM cycle the pedestal pressure gradient is not limited by kinetic ballooning modes. Any pedestal model based on pressure gradient being limited by kinetic ballooning modes needs to amended when predicting pedestals with high bootstrap current.

Unstable micro-tearing modes are found at the JET pedestal top, but they are sub-dominant to ion temperature gradient modes. They are insensitive to collisionality and stabilised by increasing density gradient.

1. INTRODUCTION

The global plasma confinement in a tokamak operating in high confinement or H-mode is largely determined by the edge pedestal pressure due to core turbulence restricting $\nabla T/T$ near the marginal stability limit[1]. Therefore, being able to predict the edge pedestal behaviour allows prediction of the achievable core pressure and the fusion power. There is strong evidence from various devices that in Type I ELMy H-mode the pedestal pressure is constrained by ideal MHD peeling-ballooning modes. When the stability limit is exceeded, the peeling-ballooning mode is thought to trigger an instability causing an ELM crash that reduces the pedestal top pressure. The stability calculations of JET [2], DIII-D [3], JT-60U [4] and ASDEX Upgrade [3] have all found plasma to be within error margin of the peeling-ballooning stability limit prior to a Type I ELM crash.

However, the peeling-ballooning constraint does not solely determine the pedestal pressure. By increasing the width of the pedestal it is possible to maintain peelingballooning stability at higher pedestal top pressure with a reduced pressure gradient. In order to uniquely predict the maximum achievable pedestal, the pedestal width also has to be constrained. One way is to find an empirical scaling for the width using dimensionless parameters from the experiments e.g. $\Delta_{ped} \sim \beta_{p,ped}^{0.5}$ [5]. This constraint is used in the EPED1 model, which combines the scaling law prediction for the width to a peeling-ballooning stability calculation for the height of the pedestal[6]. A more advanced version of EPED, EPED1.6, replaces the scaling law constraint with an ideal MHD calculation for n = 1 ballooning modes, which is used as a proxy for the stability of kinetic ballooning modes (KBM) [7]. Both the linear growth rate and the nonlinear heat flux from KBMs increase very rapidly after the stability limit is exceeded, constraining the pedestal pressure gradient below this limit [8].

In recent gyrokinetic studies of MAST plasmas, in addition to KBMs, micro-tearing modes

(MTM) were found unstable near the top of the pedestal [9, 10]. This suggests a model where the widening of the pedestal is due to MTMs in the shallow gradient region at the top of the pedestal becoming stabilised by increasing density and pressure gradients at the "knee" of the pedestal top, allowing the steep pressure gradient to increase until the KBM stability limit is reached [10].

Whilst the EPED model has been able to predict a large number of JET pedestal pressures at a 20-30% accuracy [11], some of the trends are not correctly predicted. In this paper we investigate the linear stability limit in the pedestal region of well-diagnosed ELM cycles in JET. The selected plasmas are from a density scan that show discrepancy from the EPED predictions [12]. The pedestal width dependency of $\Delta_{ped} \sim \beta_{p,ped}^{0.5}$ is not seen in the scan. Also the prediction for the pedestal pressure shows a decreasing trend for increasing density while the opposite is observed experimentally.

We try to understand the underlying causes for the discrepancies by using linear ideal MHD and gyrokinetic stability analyses. First in section 2, we construct the plasma equilibrium using the HELENA code [13] including the bootstrap current that is dominant in the edge region. HELENA also calculates the local n = ∞ ballooning stability for each flux surface. Then we use the HELENA equilibria to study the peelingballooning stability with a finite-n MHD stability code MISHKA-1 in section 3. Finally, the gyrokinetic code GS2 [14] is used to investigate the micro-stability in section 4. We determine the KBM unstable region during the ELM cycle and how well this corresponds to the region that is unstable to the ideal MHD n = ∞ ballooning modes. We will also investigate, whether unstable MTMs are found near the pedestal top.

2. EXPERIMENT AND EQUILIBRIUM RECONSTRUCTION

2.1. EQUILIBRIUM RECONSTRUCTION PROCEDURE

In order to study the MHD and gyrokinetic stability of the JET pedestal, we first need to accurately reconstruct the equilibrium. The electron density and temperature are obtained using the high resolution Thomson scattering diagnostics [15, 16]. The profiles are measured in R,Z coordinates, mapped to equilibrium poloidal flux by using the EFIT equilibrium, binned according to their timing in the ELM cycle and then the combined profiles are fitted with a mtanh-function [17] using a deconvolution technique described in [16]. Since the EFIT separatrix position is not very accurate, we adjust the radial position of the profiles so that the separatrix temperature matches with two-point power balance model [18]:

$$\alpha = \frac{-2\partial V/\partial\psi}{(2\pi)^2}\left(\frac{V}{2\pi^2 R_0}\right)^{1/2}\mu_0\frac{\partial\pi}{\partial\psi}, \qquad (1)$$

where T_{div} is the temperature at the divertor (in eV), P_{heat} is the total heating power (in MW), P_{rad} is the total radiative power from the core (in MW), $L_{||} = \pi R_0 q_{95}$ is the parallel connection length (in m), λ_q is the radial power decay length (in m), R_{OMP} is the major radius of the outer midplane (in m) and k_0 is the heat conduction. The values used in this paper are either taken from the experiment (R_0, P_{heat}, P_{rad}, q_{95},R_{OMP}) or assumed ($\lambda_q = 0.005$, $k_0 = 2000$).

For ion temperature, we have assumed that in the core $T_i = T_e$ and used two different assumptions for the pedestal, either $T_i = T_e$ or $dT_{i,ped}/d\psi = dT_{i,core}/d\psi$. It turns out that the choice of the assumption of ion temperature has little effect on the equilibrium and stability. For the Z_{eff}, which affects the bootstrap current through collisionality as well as ion density through dilution, we have used a line-integrated measurement and assumed constant value in the plasma.

The current profile is assumed to be a combination of inductively driven and bootstrap current. The bootstrap current is calculated from density and temperature profiles using formulas in [19, 20]. The inductively driven current is assumed to be fully relaxed to the neo-classical conductivity profile, which slightly overestimates the core current but has little effect on the equilibrium near the edge where the bootstrap current dominates. The plasma boundary shape is taken from EFIT. Using this information, we calculate a fixed boundary equilibrium that has a self-consistent bootstrap current with the HELENA code using the method described in [21].

To improve further the quality of the equilibrium, we redo the mapping of the profiles from real space into the flux space using the HELENA equilibrium. It turns out that the effect of this remapping on the profiles is small and the edge pressure gradient changes by less than 5%.

2.2. INVESTIGATED PLASMAS

For this study, we have chosen two high triangularity ($\delta = 0.41$) JET discharges with $I_p = 2.5$MA and $B_t = 2.7$T. The Pulse No: 79503 has high fuelling (2.6×1022e/s) and the Pulse No: 79498 has low fuelling (0.2×10^{22}e/s). The density, temperature and pressure profiles of the two plasmas during the ELM cycle are shown in Fig.1. The period right after the ELM crash (0–10% of the ELM cycle) is ignored because the data in the period is dominated by the ELM crash and not very useful for analysis. Excluding it does not change any of the conclusions presented in the paper. A more detailed discussion about the data and fitting is given in [12]. Z_{eff} is 2.0 for the low fuelling case and 1.7 for the high fuelling case.

As described in detail in [12], the pedestal behaviour between ELMs is different in these two cases. In the low fuelling plasma, both the temperature and density pedestal height increases and the width decreases during the ELM cycle resulting in an increasing pressure gradient until the ELM crash collapses the pedestal.

In the high fuelling case; the density pedestal height increases slightly while the temperature profile stays unchanged after the quick recovery following the ELM crash; initially (up to midway through the ELM cycle) the maximum pressure gradient in the pedestal increases, but then saturates and does not change for a large part of the ELM cycle. The width of the pressure profile increases very slightly during the ELM cycle. The time evolution of the pressure gradient and the pedestal width for both discharges are shown in Fig.2.

In the equilibrium reconstruction the self-consistent bootstrap current is assumed to follow the pressure profile without a delay. It has been shown that this is a good approximation for current diffusion in similar plasmas in ASDEX Upgrade [28]. The resulting toroidal current and q-profiles

are shown in Fig.3. As can be seen, the q-profile develops a flat part in the location of the maximum bootstrap current.

3. MHD STABILITY ANALYSIS

3.1. FINITE-N MHD STABILITY ANALYSIS

The finite-n MHD peeling-ballooning instabilities have been found to limit the pedestal height in Type I ELMy H-mode plasmas in several devices [6]. In this paper, we use the MISHKA-1[23] ideal MHD code to investigate the finite-n stability of the plasma during the ELM cycle. We conduct two different types of scans around the experimental MHD and Gyro-kinetic Stability of JET Pedestals 6 equilibrium. First we map the stability boundaries in $\alpha - < j_\phi >_{max}$-space. Here the normalized pressure gradient, α, is defined as [24]

$$T_{e,sep}\,[eV] = \left(T_{div}^{\frac{7}{2}} + \frac{7}{2}\,(P_{heat} - P_{rad})\,\frac{L_{\parallel}}{\lambda_q 2\pi R_{OMP} k_0} \right)^{\frac{2}{7}} \tag{2}$$

where V is the plasma volume, R_0 is the major radius and p is the pressure. $< j_\phi >_{max}$ is the maximum of the flux surface averaged toroidal current density in the pedestal region. In the scan we vary the $dp/d\psi$ and $< j_\phi >$ profiles from the experimental profile using the method described in detail in [27]. This method allows the profiles to be varied locally without introducing discontinuities.

The finite-n stability diagrams of the two discharges are shown in Fig.4. In the diagrams the color represents the growth rate, γ, of the most unstable mode and the stability boundaries are drawn for $\gamma = 0$ and $\gamma = \omega_*/2$, where ω_* is half of the maximum diamagnetic frequency for a given mode number in the pedestal.

In both cases the edge plasma starts the ELM cycle deep in the stable region. In the low fuelling case the pressure gradient and the current density keep increasing until the end of the ELM cycle, when the plasma has crossed into the unstable region. Since the pedestal width of the last time point is close to the width of the instrument function used in the fitting, the deconvolution technique used in the fitting procedure may in this particular case overestimate the gradient that would explain the last time point being relatively deep in the unstable region. In the high fuelling case the pressure gradient and the current density saturate long before the ELM crash with the edge plasma close to marginal stability. As a conclusion of the finite-n stability analysis we can say that the result is consistent with the assumption in the EPED model that the peeling-ballooning modes are the ultimate limit for the pedestal height.

3.2. N = ∞ MHD STABILITY ANALYSIS

It has been shown that the local $n = \infty$ ballooning stability, which can be calculated very quickly for an equilibrium, matches with the kinetic ballooning mode (KBM) stability calculated by a local gyrokinetic code [9]. In the analysis presented in [9] for the MAST plasma, the edge plasma is relatively cold ($T_{e,ped} < 200$ eV) resulting in a relatively collisional plasma with a small bootstrap

current peak. However, in the JET discharges analyzed in this paper the pedestal temperature is much higher ($T_{e,ped} \approx 1$keV) and the resulting bootstrap current peak is large. As was shown in Fig.3 the bootstrap current peak flattens the q-profile in the steepest pressure gradient region. The low magnetic shear allows the pedestal to access the so-called 2nd stability region. Figure 5 shows the $n = \infty$ ballooning mode stability evolution during the ELM cycle in the two analyzed JET discharges. In the graph $F = \alpha_{crit}/\alpha$, where α_{crit} is the marginally ballooning stable value of α. The flux surfaces where $F > 1$ are stable and those with $F < 1$ are unstable. As can be seen, there is a narrow band of unstable plasma between the steepest gradient and the edge. The steepest pressure gradient region is stable through the ELM cycle due to being in the 2nd stable region. This 2nd stability access of the steep pedestal region in Type-I ELMy plasmas is typical of what has been found earlier in DIII-D and JET [22, 25, 26] and is due to the strong bootstrap current peak in the pedestal. The"knee" or the top of the pedestal is also stable, but closer to the stability limit than the steepest gradient region.

We demonstrate that the $n = \infty$ stability in the steepest pressure gradient region is due to the bootstrap current peak by conducting a scan in which we vary the amount of bootstrap current included in the equilibrium reconstruction. The result shown in Fig.6 are from the equilibria at the end of the ELM cycle, but similar results are found for other time points. As can be seen the pedestal region indeed becomes unstable as the bootstrap current is reduced from the value given by the formulas in Ref. [19]. As can also be noted, the "knee" region becomes unstable with less reduction of current than is required to destabilize the steepest pressure region.

It is possible that while the steepest part of the experimental profile (after being fitted with an mtanh-function) is in the 2nd stable region due to the high bootstrap current, it has passed through the unstable region during the increase of temperature pedestal. Consequently, KBMs would have been triggered and they would have limited the local increase of the pressure gradient. The gradients would still increase in other parts of the pedestal until they become clamped by KBMs throughout the pedestal. This is the idea behind the ballooning critical pedestal (BCP) method used in the EPED 1.6 model [7]. Another possibility is that the experimental 2nd stable region move from the 1st to the 2nd stable region as the pressure gradient increases without crossing through the unstable region. In this case these regions would never become limited by the kinetic ballooning modes.

We already saw in Fig.5 that the steep pressure gradient regions of the JET pedestals do not become $n = \infty$ ballooning unstable at any point during the ELM cycle. However, during the ELM cycle, both the width of the pedestal and the location of the steepest part changes. In order to study just the effect of pedestal steepening, we conduct an artificial scan by taking the profiles of the last point of the ELM cycle and varying the height of the temperature pedestal, solving the equilibrium self-consistently with bootstrap current and recording which flux surfaces are $n = \infty$ ballooning unstable. The unstable flux surfaces for a given pedestal height are plotted in Fig.7. In the scan no unstable flux surfaces were found for pedestal pressure values lower than the values shown in the plot. This means that for both high and low fuelling plasmas the steepest pressure gradient never becomes $n = \infty$ ballooning unstable as the gradient increases, i.e. it never crosses the stability

boundary as it moves from the first to the second stable region. Only the very narrow (especially in the case of low fuelling plasma) outer region can be considered to be limited by the ballooning instability.

4. GYRO-KINETIC ANALYSIS

Finite-n MHD stability of the plasma edge stability provides hard limits that plasma cannot cross without leading to the loss of a considerable part of the plasma as happens MHD and Gyro-kinetic Stability of JET Pedestals 8 during an ELM. However, more benign turbulence driven by local micro-instabilities can also limit the edge gradients through transport. In order to be relevant for limiting the pressure gradient, the micro-instability has to have a critical value for the gradient after which its growth rate increases rapidly driving turbulence and reducing the gradient. A mode that does not have this property but is found to be unstable in the pedestal can still affect the dynamics of the pedestal evolution by slowing down the recovery of the pedestal, but does not determine the maximum achievable pressure gradient.

To study the micro-instabilities in the pedestal region during the ELM cycle in more detail, we use local gyro-kinetic analysis, and we consider modes with size of the order of ion Larmor radius, which is generally small compared to the equilibrium scale lengths. At the top of the pedestal this requirement is easily met ($L_T/\rho_i \approx 80$ and $L_n/\rho_i \approx 800$), but in the steep gradient region the gyrokinetic expansion parameter is larger (both L_n/ρ_i and $L_T/\rho_i \approx 10–20$). We will now look at local gyrokinetic stability in both of these regions.

4.1. GYROKINETIC STABILITY IN THE STEEP GRADIENT REGION

In the previous section we found that the JET pedestals are in the 2nd stable region for $n = \infty$ ideal MHD ballooning modes. It is well known for long that the ideal MHD ballooning modes and kinetic ballooning modes have very similar drive mechanisms [29]. In MAST pedestal the ideal MHD $n = \infty$ stability has been found to be a good proxy for kinetic ballooning mode (KBM) stability calculated by a local gyro-kinetic code when the plasma is in the 1st stable region [9]. We will now test if this is true also for the JET pedestal that is in the 2nd stable region for ideal MHD ballooning modes. For this analysis we use the local electro-magnetic GS2 code [14]. Both the ions and electrons are treated kinetically and the collisions are taken into account. The effect of sheared flow, while important for modes with growth rates similar to the shearing rate, may be less important for KBMs because once the plasmas crosses the stability boundary for KBMs, the growth rate increases very rapidly [8, 30] resulting only in a small increase in the critical pressure gradient. Therefore, the flow shear is neglected in this analysis. Future studies are planned to include the effect of the flow shear.

The linear gyro-kinetic stability analysis at $k_\theta\rho_i < 0.2$ (k_θ is the poloidal wave number and ρ_i is the ion Larmor radius) finds no kinetic ballooning modes (KBM) in the JET pedestals. This agrees with the ideal MHD $n = \infty$ stability described earlier. At higher k_θ ($0.2 < k_\theta\rho_i < 2$) we find ion temperature gradient (ITG) modes and at even higher k_θ ($k_\theta > 5$) electron temperature gradient (ETG) modes.

Both of these are electro-static and their growth rate depends very weakly on the plasma (the ratio of plasma pressure to magnetic energy). Also they are not destabilized by increasing density gradient making them unlikely candidates for limiting the pedestal density gradient. Therefore, while it is possible that these modes play a role in the limiting of the pedestal temperature gradient and slowing down the pedestal recovery, in this paper we concentrate on KBMs that are destabilized by increasing pressure gradient and have very high growth rates producing a lot of turbulent transport once the stability limit is exceeded [31].

We scan the plasma β in GS2 (i.e. not solving for a new self-consistent equilibrium using HELENA) to find the stability limit for KBMs in JET pedestals. As can be seen in Fig.8, the amount by which β must be increased in order to destabilize KBMs matches very well with the F parameter in the $n = \infty$ ideal MHD analysis throughout the pedestal region. So, while the validity of the gyrokinetic theory in the pedestal region is marginal due to small L_n/ρ_i and L_T/ρ_i values, the numerical results for KBMs still agree very well with the ideal MHD results. We can also see that the regions closest to the stability limit are the bottom of the pedestal ($\psi \approx 0.99$) and the "knee" of the pedestal ($\psi \approx 0.94$ in high fuelling case and $\psi \approx 0.96$ in the low fuelling case). The steepest part of the pedestal is very stable for KBMs.

The reason for the good stability for KBMs in the pedestal is the large bootstrap current that lowers the flux-surface averaged magnetic shear in the steep pressure gradient region. As was shown in the previous section, reducing the bootstrap current that included in the equilibrium reconstruction destabilizes the local $n = \infty$ ballooning modes. Exactly the same happens with the KBMs in a gyrokinetic simulation. Figure 9 shows the KBM growth rate in the pedestal region when no bootstrap current has been taken into account. In the low fuelling case, the KBM growth rate has two peaks: one between the edge and the maximum pressure gradient and the other between the top of the pedestal and the maximum pressure gradient. These peaks match very well with the ideal MHD $n = \infty$ ballooning unstable regions, i.e. the most $n = \infty$ ballooning unstable regions have also the highest growth rates for KBMs. In the high fuelling case, the KBM growth rate peaks just outside the steepest gradient region. Also in this case the KBM unstable region match very well with the region unstable to ideal MHD ballooning modes.

4.2. GYROKINETIC STABILITY AT THE PEDESTAL TOP

In a gyro-kinetic analysis of the MAST tokamak, it was found that the plateau region at the top of the pedestal is unstable to micro-tearing modes (MTM) [32, 10, 33]. The identification of the micro-tearing modes in the JET pedestal top is made more difficult by other unstable micro-instabilities. In the JET pedestal top, ITG modes are the dominant instability. In order to identify possible sub-dominant micro-tearing modes, we make the equilibrium up-down symmetric and in GS2 suppress even parity modes such as the ITG. Changing the plasma shape to up-down symmetric has very little effect on the growth rates of the dominant mode. When the ITG modes are suppressed, we find sub-dominant odd parity micro-tearing modes. Figure 10 shows the growth rates of the ITG

(unsuppressed case) and MTM (when ITG is suppressed) at the "knee" of the pedestal for both cases at the end of the ELM cycle. The growth rate spectra for different time points is qualitatively similar. Similar to what was found in MAST [10, 32] and unlike micro-tearing modes found in the core, the mode structure of the pedestal top micro-tearing mode is not very extended along the field lines as shown in Fig.11. We also find that this mode is relatively insensitive to the collisionality (growth rate increases slightly with decreasing collisionality) and is unstable even when collisions are ignored in the gyrokinetic simulation. The growth rate of the MTM at the pedestal top decreases with increasing density gradient and increases with increasing temperature gradient as in [10, 32, 33]. The MTM stabilization by the density gradient means that MTMs can contribute to the transport of the pedestal top region until they are suppressed by the increasing edge density gradient as described in [10].

CONCLUSIONS

The finite-n MHD and stability analyses presented in this paper suggest that the carefully reconstructed experimental pedestals of both high and low fuelling JET Type I ELMy plasmas are limited by peeling-ballooning modes within experimental uncertainty at the end of the ELM cycle. This confirms previous results from JET and various other devices and is consistent with the EPED model assumption the peeling-ballooning modes limit the pedestal. In the early part of the ELM cycle both cases are stable to peelingballooning modes. The pedestal in the high fuelling case is found to saturate near the stability boundary around half-way through the ELM cycle, while in the low fuelling case the pedestal pressure gradient keeps increasing until the ELM crash.

In the pedestal region, the stability boundaries obtained using local ideal MHD $n = \infty$ ballooning mode analysis and local linear gyro-kinetic analysis for kinetic ballooning modes show very good correspondence. This is consistent with the MHD $n = \infty$ ballooning mode stability providing a reasonable proxy for the stability of kinetic ballooning modes. However, in the analyzed JET discharges most of the pedestal region is found to be stable to both of these modes due to reduced magnetic shear caused by high bootstrap current in the steep pressure gradient region giving access to 2nd stability. In a self-consistent pedestal height scan the steepest part of the pedestal moves from the 1st to the 2nd stable region without crossing the unstable region.

The experimental observation of increasing pressure gradient in the case of the low fuelling plasma and the MHD and gyro-kinetic stability analyses suggest that the edge pedestal gradient in JET is not limited by kinetic ballooning modes during the ELM cycle. Further, the narrowing of the pedestal through the ELM cycle in the low fuelling case indicates a different type of ELM cycle to that seen in DIII-D and MAST where the pedestal widens with a constant maximum pressure gradient [34, 9]. The analysis also indicates KBMs do not limit the pressure gradient in pedestals with large edge bootstrap current peak and low magnetic shear as expected in ITER [35]. The sensitivity of the KBM stability to the amount of bootstrap current, however also points to the need for accurate measurement of the edge current profile to validate the neoclassical models for bootstrap current used in the calculations.

The experiment was found to be consistent with the pedestal being ultimately limited by peeling-ballooning modes. The width dependency of the peeling-ballooning mode limit for the pedestal top pressure is relatively weak [7, 35]. Therefore, it may not be necessary to get the width exactly right in order to have a reasonable prediction for the pedestal height.

Gyro-kinetic analysis also found micro-tearing modes at the JET pedestal top with similar features to those found earlier in the MAST pedestal top. However, in JET the micro-tearing modes are sub-dominant to ITG modes, but could nevertheless play a role in the pedestal dynamics.

The local gyrokinetic analysis has its limitations when the ion Larmor radius approaches the equilibrium scale lengths. It is possible that the equilibria with a high bootstrap current peak and low shear at the maximum pressure gradient are locally stable for KBMs but become unstable when finite radial width of the mode is taken into account limiting the pressure gradient. Such an analysis is beyond the scope of this paper and will be considered in future work.

ACKNOWLEDGEMENTS

This work was partly funded by the RCUK Energy Programme under grant EP/I501045 and the European Communities under the contract of Association between EURATOM and CCFE and carried out within the framework of the European Fusion Development Agreement. The views and opinions expressed herein do not necessarily reflect those of the European Commission. The gyrokinetic calculations were done on HECToR supercomputer (EPSRC grant EP/H002081/1).

REFERENCES

[1]. Ryter F. et al., Plasma Physics and Controlled Fusion **43** (2001) A323
[2]. Saarelma S. et al., Plasma Physics and Controlled Fusion **51** (2009) 035001
[3]. Snyder P.B., et al. Nuclear Fusion **44** (2004) 320
[4]. Saibene G., et al., Nuclear Fusion **47** (2007) 969
[5]. Beurskens M.N.A. et al., Physics of Plasmas **18**, 056120 (2011)
[6]. Snyder P.B. et al., Nuclear Fusion **49** (2009) 085035
[7]. Snyder P.B. et al., Nuclear Fusion **51** (2011) 103016
[8]. Snyder P.B. and G.W. Hammett, Physics of Plasmas **8** (2001) 744
[9]. Dickinson D. et al., Plasma Physics and Controlled Fusion **53** (2011) 115010
[10]. Dickinson D. et al., Physical Review Letters **108**,
[11]. Beurskens M.N.A. et al., Nuclear Fusion **53**, 013001 (2013)
[12]. Leyland M.J. et al., in preparation for submission to Nuclear Fusion
[13]. Huysmans G.T.A., Goedbloed J.P., Kerner W.O.K., Computational Physics (Proc. Int. Conf. Amsterdam, 1991),World Scientific Publishing, Singapore (1991) 371
[14]. Kotschenreuther M., et al., Computational Physics Communication **88** (1995) 128
[15]. Pasqualotto R. et al., Review of Scientific Instruments **75**, (2004) 3891
[16]. Frassinetti L., et al., Review of Scientific Instruments, **83** (2012) 013506

[17]. Groebner R. J. et al., Plasma Physics and Controlled Fusion **44**, (2002) A265
[18]. Kallenbach A., et al., Journal of Nuclear Materials **337-339**, (2005), 381
[19]. Sauter O., Angioni C., Lin-Liu Y.R., Physics of Plasmas, **6** (1999) 2834 MHD and Gyro-kinetic Stability of JET Pedestals 12
[20]. Sauter O., Angioni C., Lin-Liu Y.R., Physics of Plasmas, **9** (2002) 5140
[21]. Saarelma S. et al., Plasma Physics and Controlled Fusion **51** (2009) 035001
[22]. Miller R.L. et al., Plasma Physics and Controlled Fusion **40** (1998) 753
[23]. Mikhailovskii A.B. et al., Plasma Physics Report **23** (1997) 844
[24]. Miller R.L., et al., Physics of Plasmas **5** (1998) 973
[25]. Lao L.L. et al., Nuclear Fusion **39** (1999) 1785
[26]. Lönnroth J-S et al., Plasma Physics and Controlled Fusion **46** (2004) 767 (2012) 135002
[27]. Saarelma S. et al., Nuclear Fusion **52** (2012) 103020
[28]. Burckhart A., et al., Plasma Physics and Controlled Fusion **52** (2010) 105010
[29]. Kotschenreuther M., Physics of Fluids **29** (1986) 2898
[30]. Roach C.M. et al., Plasma Physics and Controlled Fusion **47** (2005) B323
[31]. Rewoldt G. et al., Physics of Fluids **30** (1987) 807
[32]. Dickinson D. et al., submitted to Plasma Physics and Controlled Fusion, arXiv:1209.3695v1
[33]. Roach C.M. et al., in preparation for submission to Nuclear Fusion.
[34]. Groebner R.J. et al., Nuclear Fusion **50** (2010) 064002
[35]. Saarelma S. et al., Nuclear Fusion **52** (2012) 103020

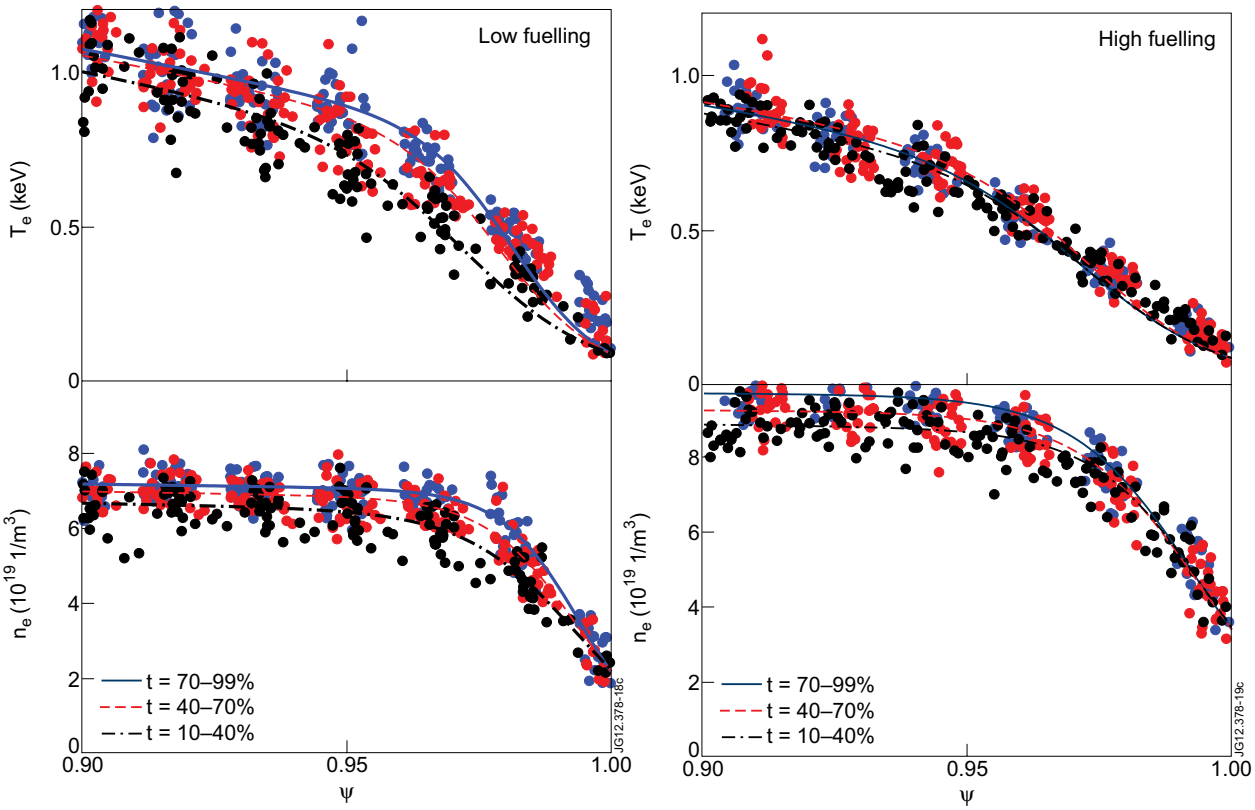

Figure 1: The density and temperature profile evolution during the ELM cycle in high (left) and low (right) fuelling JET discharges. The labels represent the normalized time in the ELM cycle.

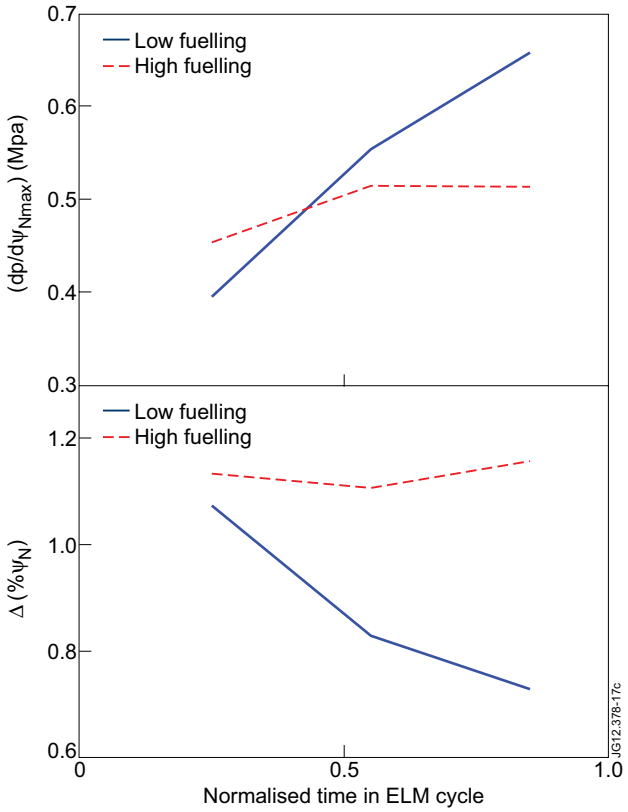

Figure 2: The time evolution of the maximum of the pedestal pressure gradient and the pedestal width during the ELM cycle in the high and low fuelling JET discharges.

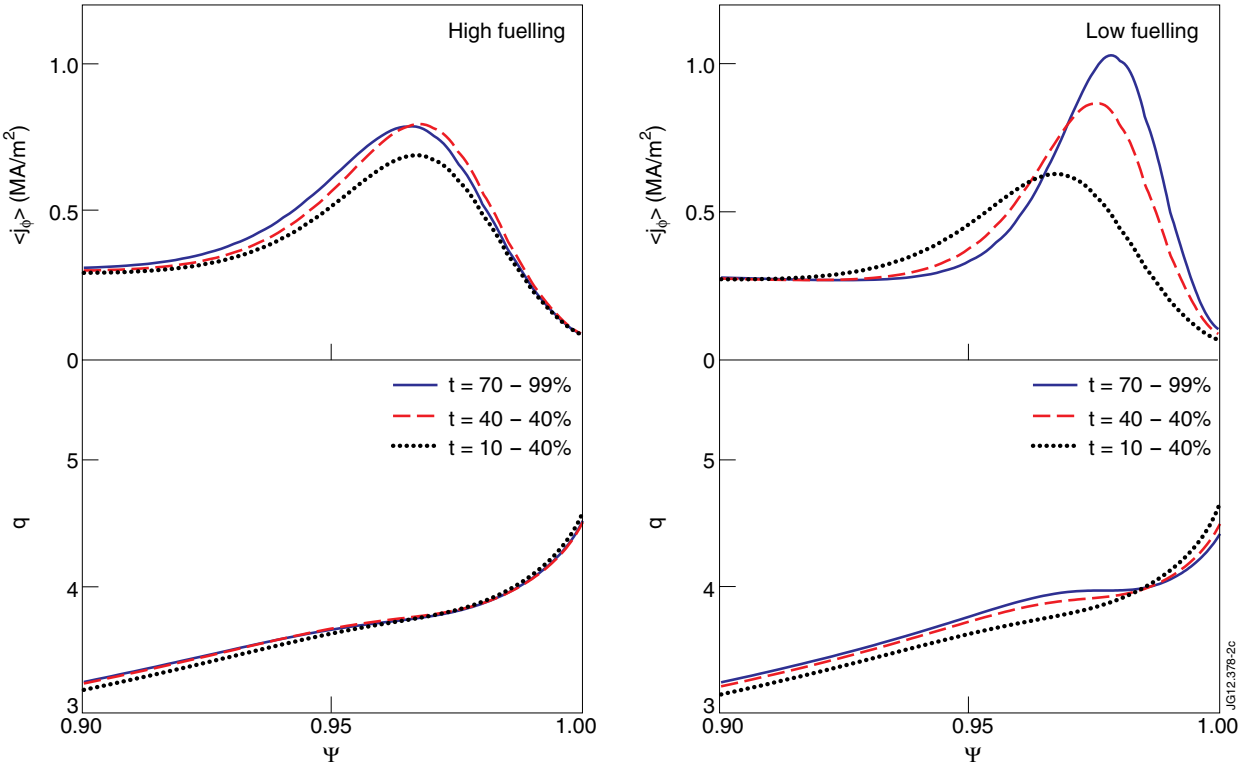

Figure 3. The flux surface averaged toroidal current and q- profile evolution during the ELM cycle in high (left) and low (right) fuelling JET discharges. The labels represent the normalized time in the ELM cycle.

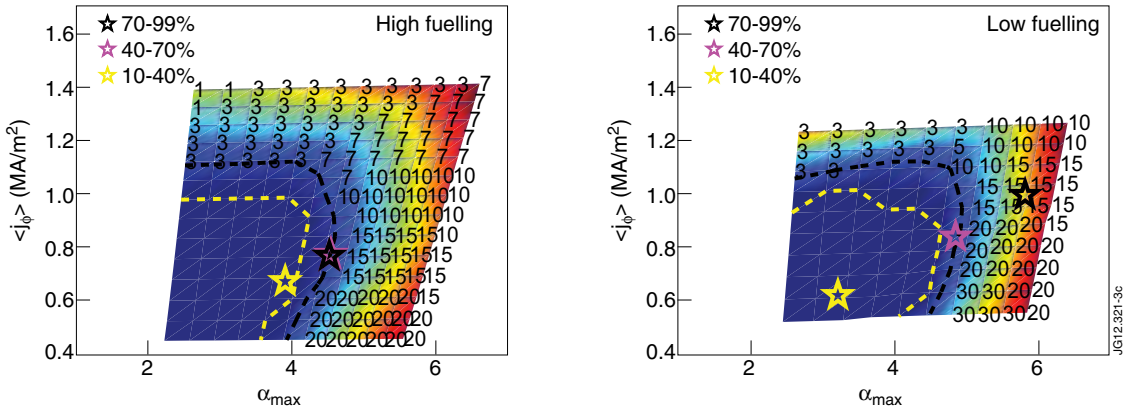

Figure 4: The peeling-ballooning mode stability diagrams for the high fuelling (left) and low fuelling (right) plasmas during the ELM cycle. The color represents the growth rate of the fastest growing mode (blue is stable) and the numbers the toroidal mode number of the most unstable mode. The dashed lines shows the stability limit at $\gamma > \omega*/2$ (black) and $\gamma > 0$ (yellow). The stars show the position of the experimental equilibrium during the ELM cycle.

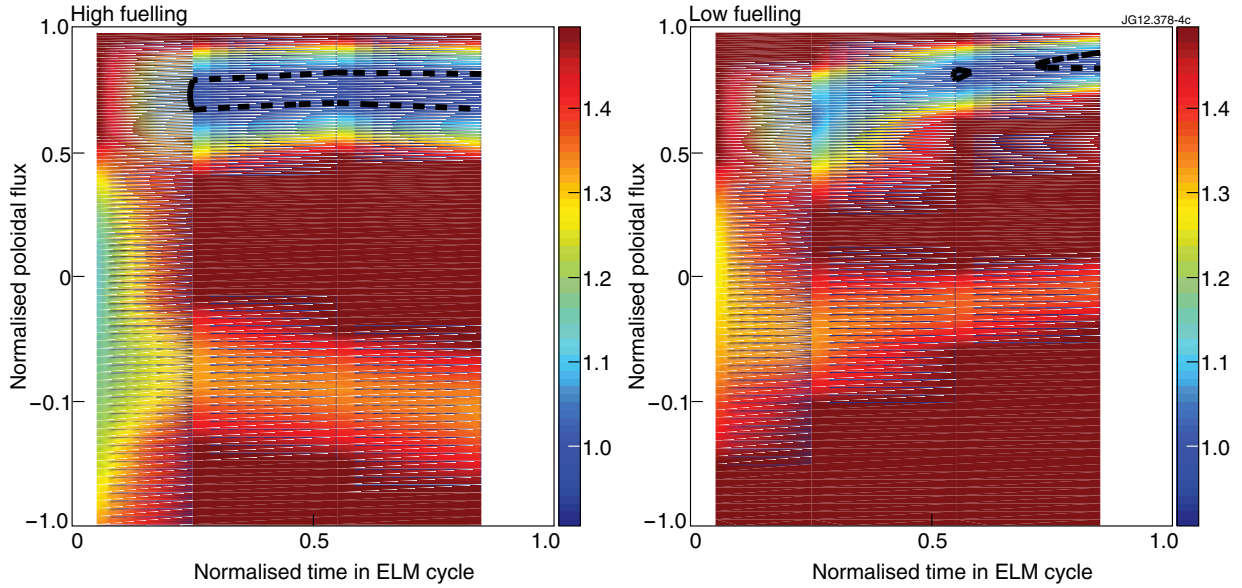

Figure 5: The n = ∞ ballooning stability during the ELM cycle in the edge region for the high (left) and low (right) fuelling cases. The colors represent the increase of pressure gradient needed to make the corresponding flux surface unstable, i.e. regions below unity are unstable and above unity stable. The dashed line shows the region of marginal stability.

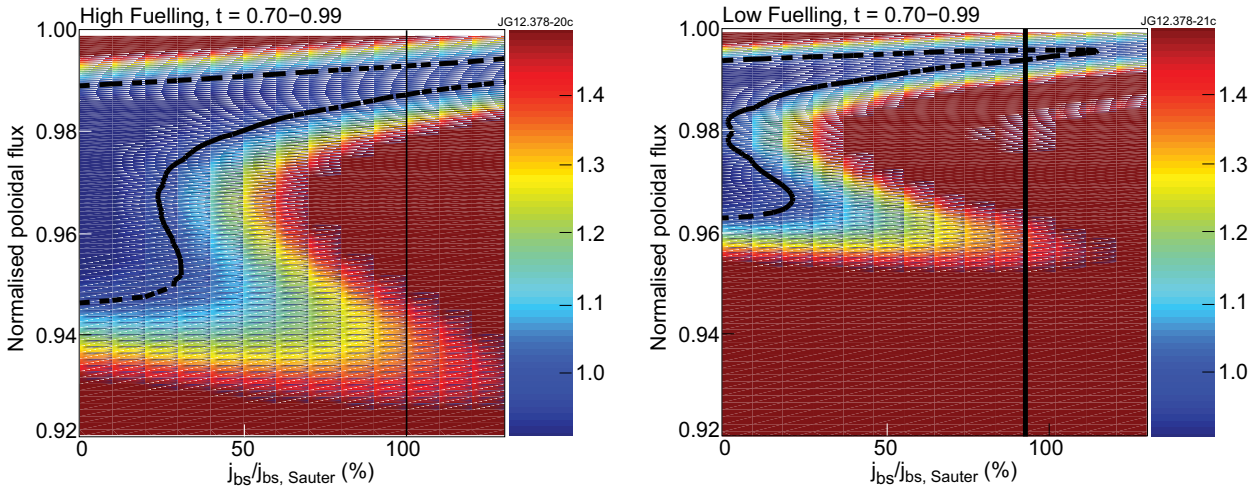

Figure 6: The n = ∞ ballooning stability as a function of bootstrap current taken into account in the equilibrium reconstruction for the pedestal region of high (left) and low (right) fuelling case at the end of the ELM cycle. The colors represent the stability (blue unstable, red stable) and the dashed black line shows the boundary of marginal stability. The vertical line represents the equilibrium with full bootstrap current given by the formula [19].

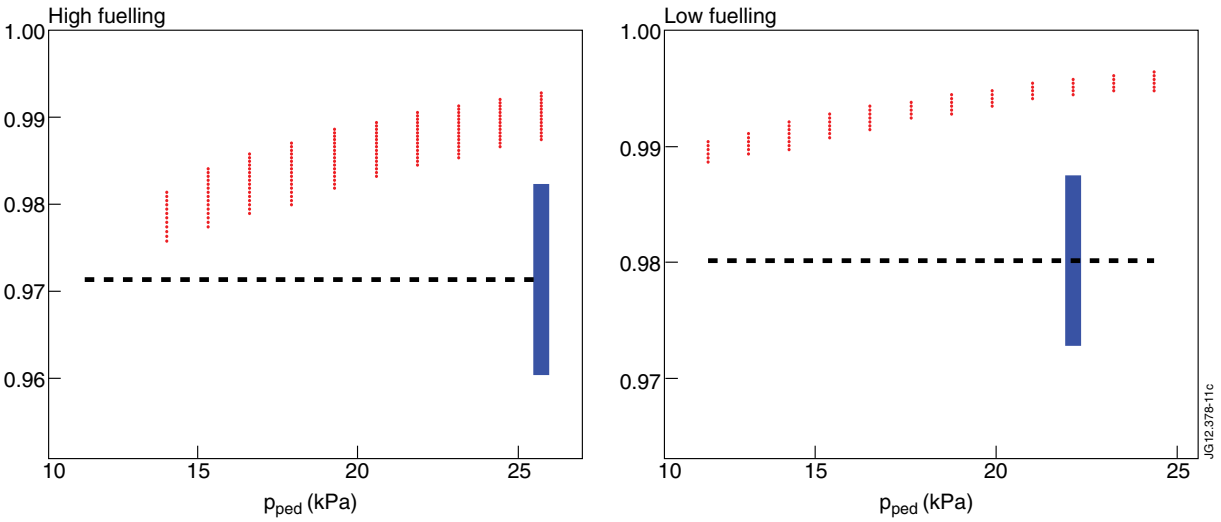

Figure 7. The n = ∞ ballooning unstable region in high (left) and low fuelling (right) cases when the pedestal top temperature is varied self-consistently. The red dots show the ballooning unstable flux surfaces. The blue line represents the region of the pressure pedestal from 25% to 75% of the height and is placed at the value of the experimental pedestal height. The black dashed line shows the steepest gradient location.

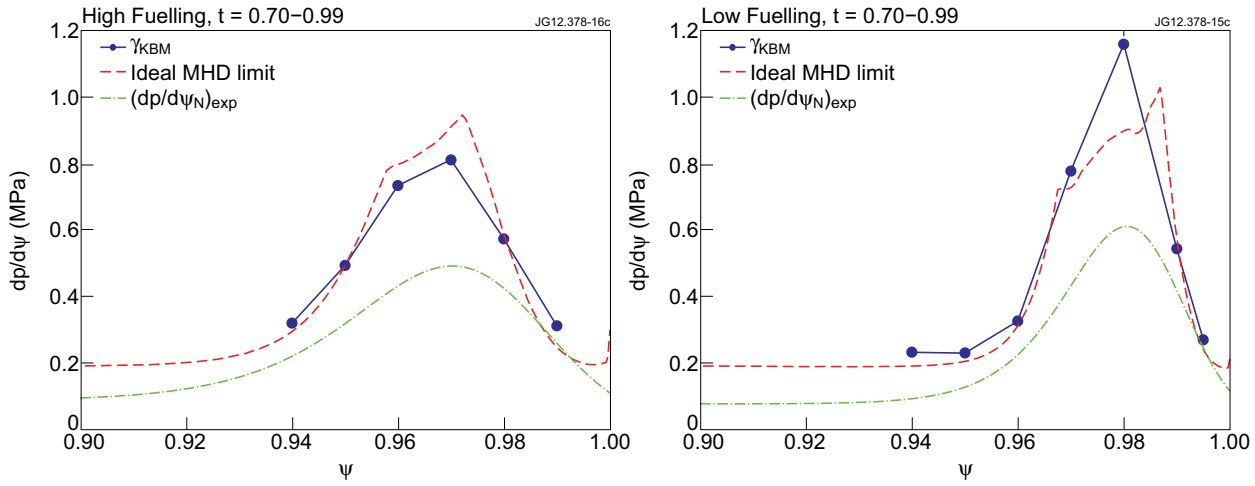

Figure 8. The gyro-kinetic stability limit of KBMs (solid blue line) in high (left) and low (right) fuelling pedestals at the end of the ELM cycle as a function of poloidal flux. For comparison, the n = ∞ ideal MHD ballooning stability limit (dashed red line) and the experimental pressure gradient (dotted magenta line) are also shown. The stability limits represent the value the pressure gradient can be increased before becoming unstable.

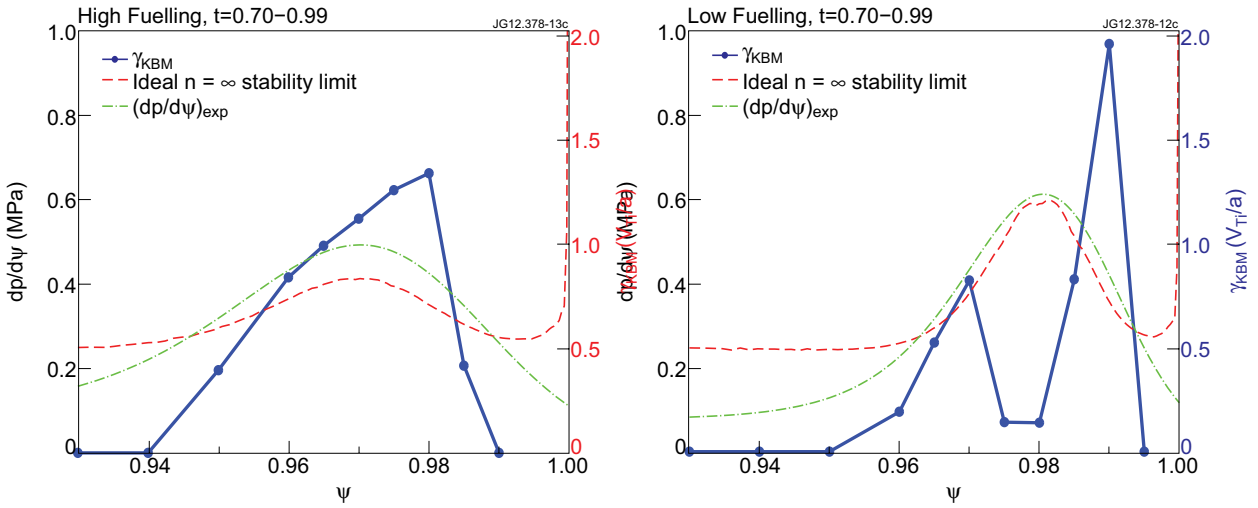

Figure 9: The growth rate of the kinetic ballooning mode (solid blue line, y-axis on the right) at the end of the ELM cycle in the edge region of high (left) and low (right) fuelling case with no bootstrap current used in the equilibrium reconstruction. Also shown is the n = ∞ ballooning stability limit (dashed red line, y-axis on the left) and the normalized pressure gradient (dash-dot magenta line, y-axis on the left).

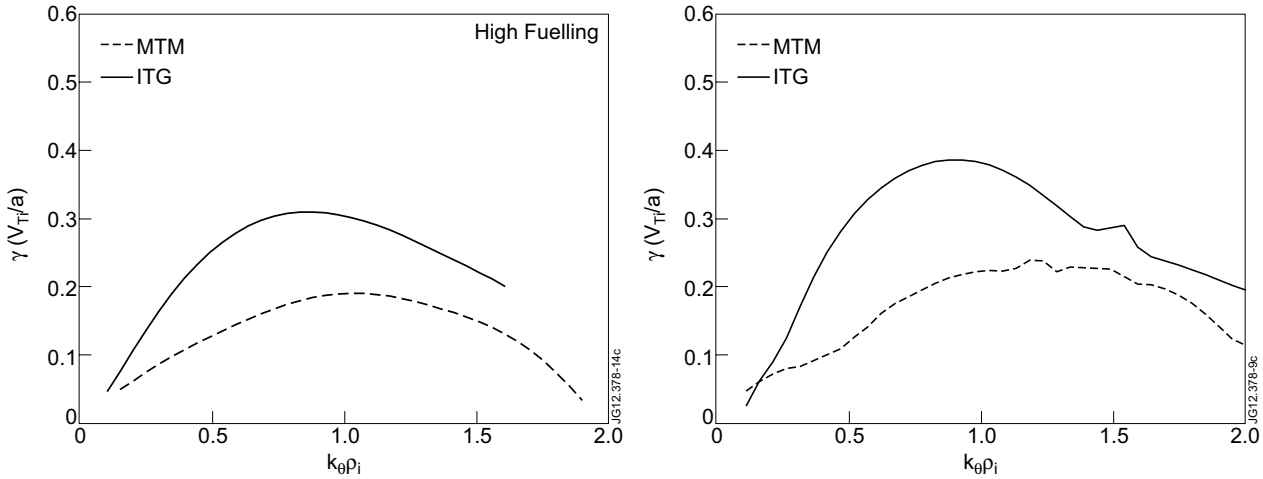

Figure 10: The growth rate spectrum of MTM and ITG modes in high (left) and low (right) fuelling case at the pedestal "knee" at the end of the ELM cycle.

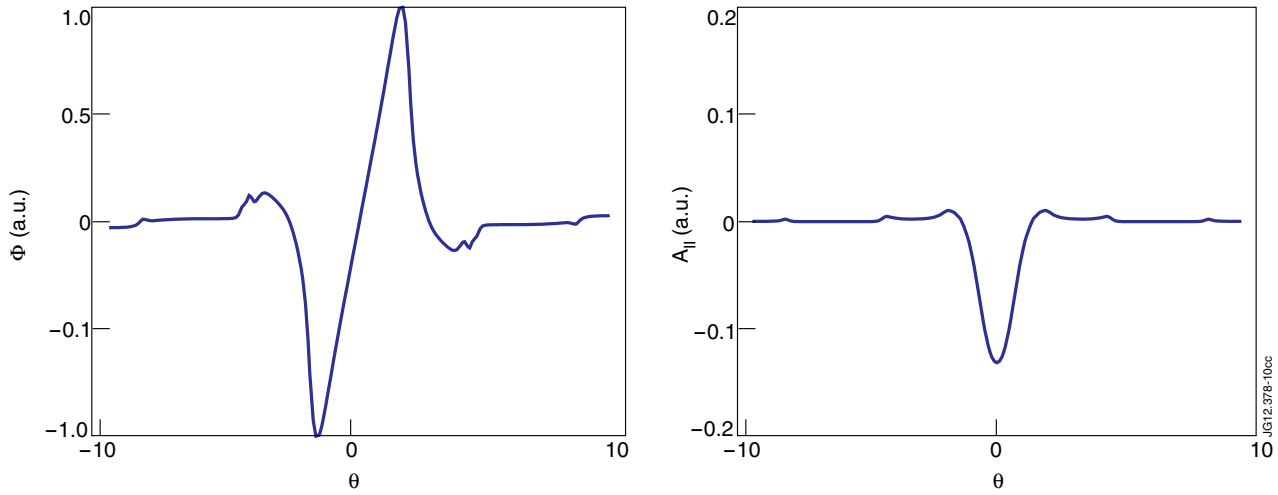

Figure 11: The eigenfunctions of electrostatic potential and parallel magnetic vector potential $A_{//}$ along the ballooning angle θ for the $k_y\rho_i = 0.37$ micro-tearing mode at the JET pedestal top.